Supplementary Information for:

Nano-alignment in semiconducting polymer films:

A path to achieve high current density and brightness in organic light emitting transistors

Mujeeb Ullah,*[,1] Khalid Muhieddine,[1] Robert Wawrzinek,[1] Jun Li,[2] Shih-Chun Lo,*[,3]

Ebinazar B. Namdas*[,1]

[1] Centre for Organic Photonics & Electronics, School of Mathematics and Physics, The University of Queensland, Brisbane, QLD 4072, Australia.

[2] Institute of Materials Research and Engineering (IMRE), Research Link, Singapore.

[3] Centre for Organic Photonics & Electronics, School of Chemistry and Molecular Biosciences, The University of Queensland, Brisbane, QLD 4072, Australia.

*Correspondence to: mujeeb.ullah@uq.edu.au, s.lo@uq.edu.au, e.namdas@uq.edu.au

Reliability factor and effective mobility calculation

EQE and Brightness Measurements

Figures S1a,b,c: EQE Calculation.

Figure S2: Device fabrication.

Figure S3: Chemical structures of DPP-DTT, Super Yellow and PCAN.

Figure S4: Capacitance *versus* scratches on SiNx dielectric.

Figure S5a: Output characteristics of SY-LEFETs.

Figure S5b: Single slope fitting of SQRT(I_{DS}) *versus* V_{GS} data of SY and PCAN based LEFETs.

Figure S6: EQE *versus* current density in SY based LEEFTs.

Figure S7: Output characteristics of PCAN-LEFETs.

Figure S8: EQE *versus* current density in PCAN based LEEFTs.

Figure S9: Electroluminescence and photoluminescence spectra of SY based LEEFTs and PCAN based LEFETs.

Figure 10: Charge transport and injection mechanism and their relative energy levels**:** (a) SY based LEEFTs; (b) PCAN based LEFETs.

Figure S11: Transmission of electron injecting electrode TPBI/Sm/Al.

Table S1: Comparison of yellow-green LEFETs in Literature.

Table S2: Comparison of blue LEFET in Literature.

References.

Reliability factor and effective mobility calculation:

The measurement reliability factor, r, is determines the behaviour of reported FETs follows the physics of the simple linear increase of conductivity with carrier density under the assumption of a constant mobility and negligible threshold voltage. It is defined as the ratio of the maximum channel conductivity experimentally achieved in a FET at the maximum gate voltage to the maximum channel conductivity expected in a correctly functioning ideal FET with the calculated carrier mobility μ and identical other device parameters at the same maximum gate voltage. Reliability factor, r can be calculated from the calculated μ, the stated device parameters and the FET characteristics. In the saturation regime, it is easy to show that the reliability factor is:

$$r_{sat} = \left[\frac{\sqrt{|I_{SD}|^{max}} - \sqrt{|I_{SD}|^{0}}}{|V_{GS}|^{max}}\right]^2 \Bigg/ \left[\frac{WC_i}{2L}\ \mu_{sat}\right]_{calculate} = \left[\frac{\sqrt{|I_{SD}|^{max}} - \sqrt{|I_{SD}|^{0}}}{|V_{GS}|^{max}}\right]^2 \Bigg/ \left[\frac{\partial\sqrt{|I_{SD}|}}{V_{GS}}\right]^2_{calculated} \qquad \text{(a)}$$

Here, μ_{sat} is the calculated mobility, L, W and C_i are the device parameters, and $|I_{SD}|^{max}$ is the experimental maximum source–drain current reached at the maximum gate voltage $|V_{GS}|^{max}$. And $|I_{SD}|^{0}$ denotes the source–drain current at $V_{GS} = 0$.

The effective mobility is calculated from the reliability factor, where reliability factor is 100%. The effective mobility can be also calculated from reliability factor and claim mobility from the equation, $\mu_{eff} = r \times \mu_{claimed}$.

EQE and Brightness measurements:

Brightness measurements:

The optical characteristics of the devices throughout this study their emission was measured using a photomultiplier tube (PMT, Hamamatsu H10721-20) which was calibrated by a luminance meter (Konica Minolta LS100) and converted into a corresponding current. This had been done using a Super Yellow based OLED with a known area and brightness. Using these known values, the photocurrent for devices could be converted to a brightness value.

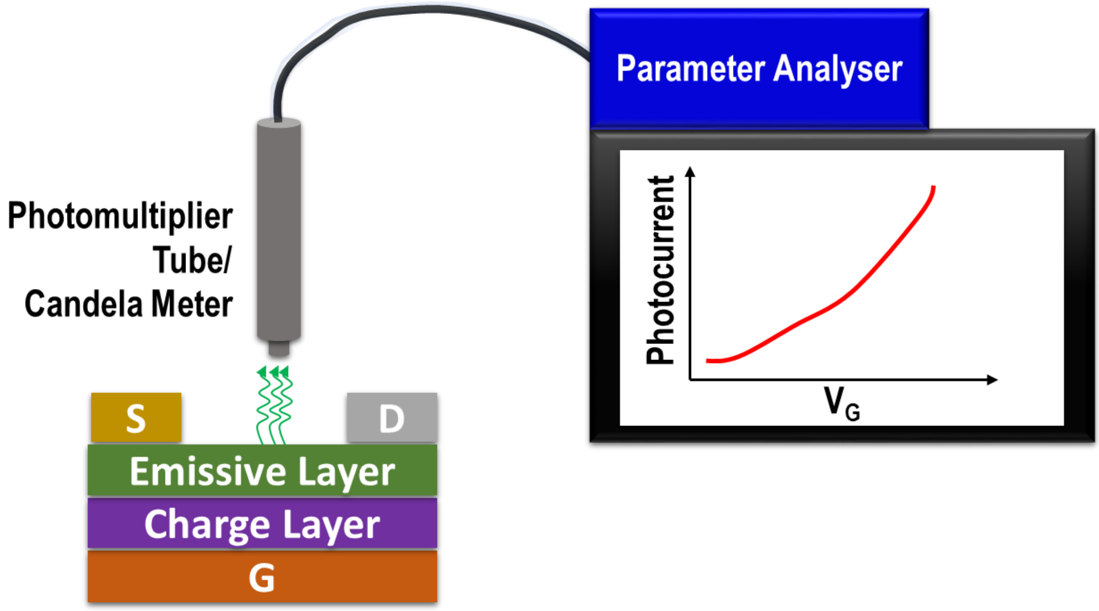

Figure S1a: A schematic of the use of the spectrometer to determine the evolution of the brightness of the device with applied gate voltage. The photomultiplier tube converts the light detected by the photodetector into an equivalent current which can be converted into a brightness.

The control OLED gave a recorded photocurrent of 71 nA per cd/m^2 and had an area of 0.92 mm^2. The calibration curve of the PMT with the OLED can be seen in **Figure S1b**. To note is that the linearity for the gain setting of 0.4 held up to approximately 600 cd/m^2. For higher values (> 600 cd/m^2) a lower gain of 0.3 was used to obtain a calibration curve. In all measurements, the distance between the PMT and the substrate was kept at a constant 1 cm to maintain a fixed solid angle.

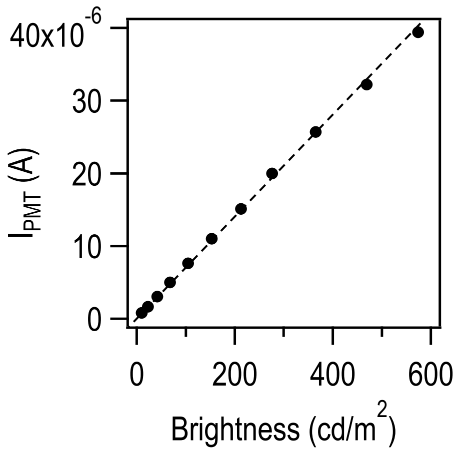

Figure S1b: The calibration curve for the photomultiplier tube with the Super Yellow OLED. The markers represent the experimental data and the line the linear fit

To calculate the brightness of the device (at 0.4 gain) a conversion factor was set up as follows:

$$Br_{DEVICE} = \frac{1}{71\,nA} \cdot \frac{0.92\,mm^2}{A_{DEVICE}} \qquad \textbf{(1)}$$

where Br_{DEVICE} is the brightness of the device and A_{DEVICE} is the area of emission. This could be calculated employing a cross-sectional histogram of the device's micrograph and extrapolation using the known dimensions of the shadow masks used for the corresponding electrode.

EQE measurements:

The emission was assumed to be Lambertian *i.e.*, with an intensity directly proportional to cos(θ) where θ is the viewing angle. Hence, taking the normal of the device as the maximum, the luminous flux Φ_{LUM} – energy emitted from the device per unit time – was then be calculated as:

$$\Phi_{LUM} = \int_0^{\frac{\pi}{2}} 2 \cdot \pi \cdot L_0 \cdot \cos\theta \cdot \sin\theta \, d\theta \qquad \textbf{(2)}$$

where θ is the angle from the normal at which the light is detected and L_0 is the brightness (in cd/m^2) of the emission. This then simplifies to:

$$\Phi_{LUM} = \pi \cdot L_0 \cdot A_{DEVICE} \qquad \textbf{(3)}$$

where A_{DEVICE} is the area of the emission and determines the final unit of Φ_{LUM} which is lumens (lm).

Because not all wavelengths are detected equally, a measurement was required to weight the spectral components of the measured light according to their detectivity by the human eye. This was done using the human eye response curve, which at the peak of sensitivity (555 nm) has a flux of 683 lm/W. The measured flux could then be related to the power following the weighted scheme:

$$\frac{\Phi_{LUM}}{Power} = 683 \frac{\int ER(\lambda) \cdot El(\lambda) d\lambda}{\int El(\lambda) d\lambda} \qquad \textbf{(4)}$$

where the top term on the right is the area under the electroluminescence curve $El(\lambda)$ weighted by the eye response curve $ER(\lambda)$ and the bottom term is the area under the electroluminescence curve $El(\lambda)$. These curves were all normalised prior to calculation and the eye response curve is shown in **Figure S1c**. This was then rearranged to find the power using the known Φ_{LUM} from the previous step.

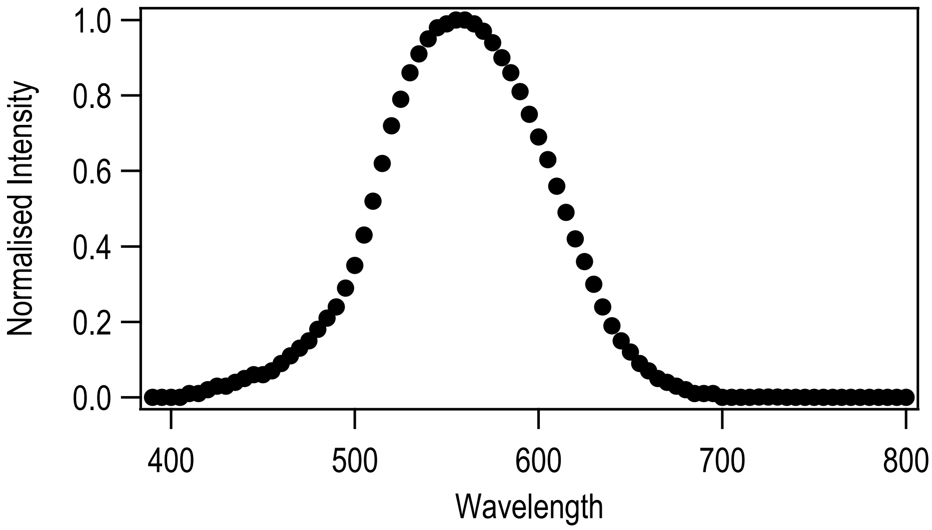

Figure S1c: The normalised Eye Response curve, indicating the sensitivity of the human eye to particular wavelengths of light.

Using the determined *Power*, the number of photons emitted from the device could then be calculated. It is known that the energy of *n* photons is:

$$E = \frac{n \cdot h \cdot c}{\lambda} \qquad \textbf{(5)}$$

where c is the speed of light, h is Planck's constant and λ is the wavelength of the light measured. For a range of wavelengths, at which devices are measured, the centroid wavelength can be calculated as follows:

$$\lambda_{CEN} = \frac{\int El(\lambda) \cdot \lambda \, d\lambda}{\int El(\lambda) d\lambda} \qquad \textbf{(6)}$$

This then allows for *n* to be calculated as:

$$n = \frac{\int El(\lambda) \cdot \lambda \, d\lambda}{\int El(\lambda) d\lambda} \cdot \frac{1}{hc} \cdot Power \qquad \textbf{(7)}$$

n is here the number of photons emitted per second, hence allowing us to convert the *E* into *Power*.

Once the number of photons emitted per second had been calculated the next step was to focus on the charge carriers. In the case this study's devices the dominant charge carriers were electrons. In order to calculate the number of electrons injected and flowing through the device per second, the source drain current was divided by the fundamental charge of an electron.

The EQE could then finally be calculated as the ratio of the number of photons emitted from the device per second (n_{ph}) to that of the number of electrons injected into the device (n_e) as follows:

$$EQE = \frac{n_{ph}}{n_e} \qquad \textbf{(8)}$$

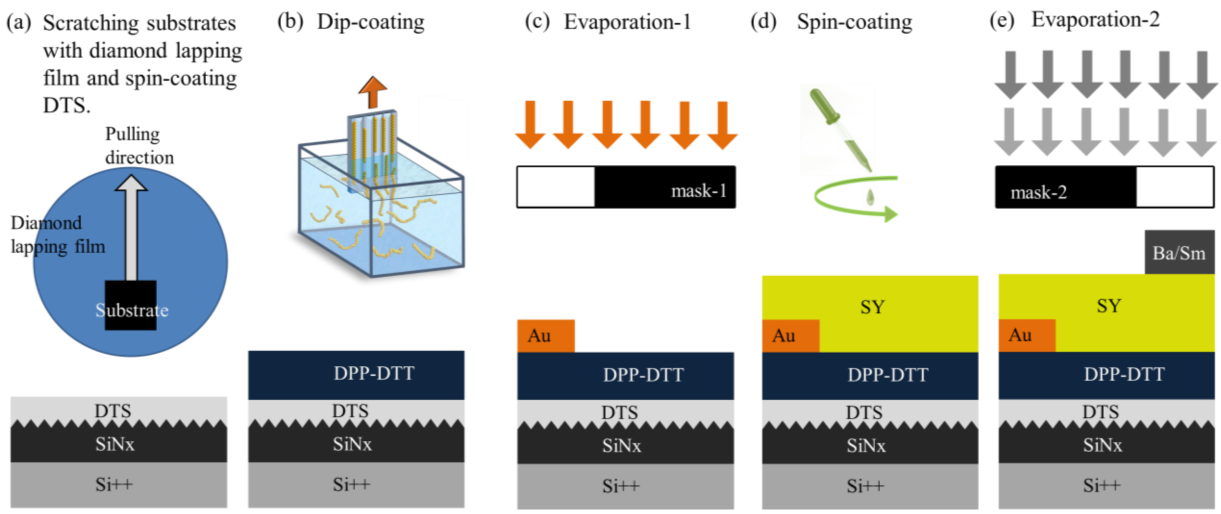

Figure S2: Device fabrication: (a) scratching the substrates using diamond lapping film; (b) dip-coating of DPP-DTT films; (c) evaporation of hole injecting electrode; (d) spin-coating and (e) evaporation of electron injecting electrode.

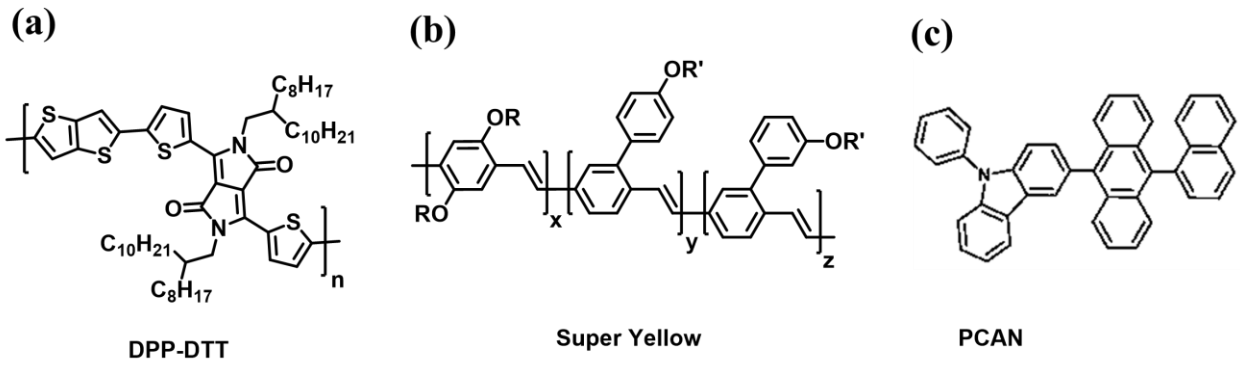

Figure S3: Chemical structures of (a) DPP-DTT; (b) Super Yellow (SY); (c) PCAN.

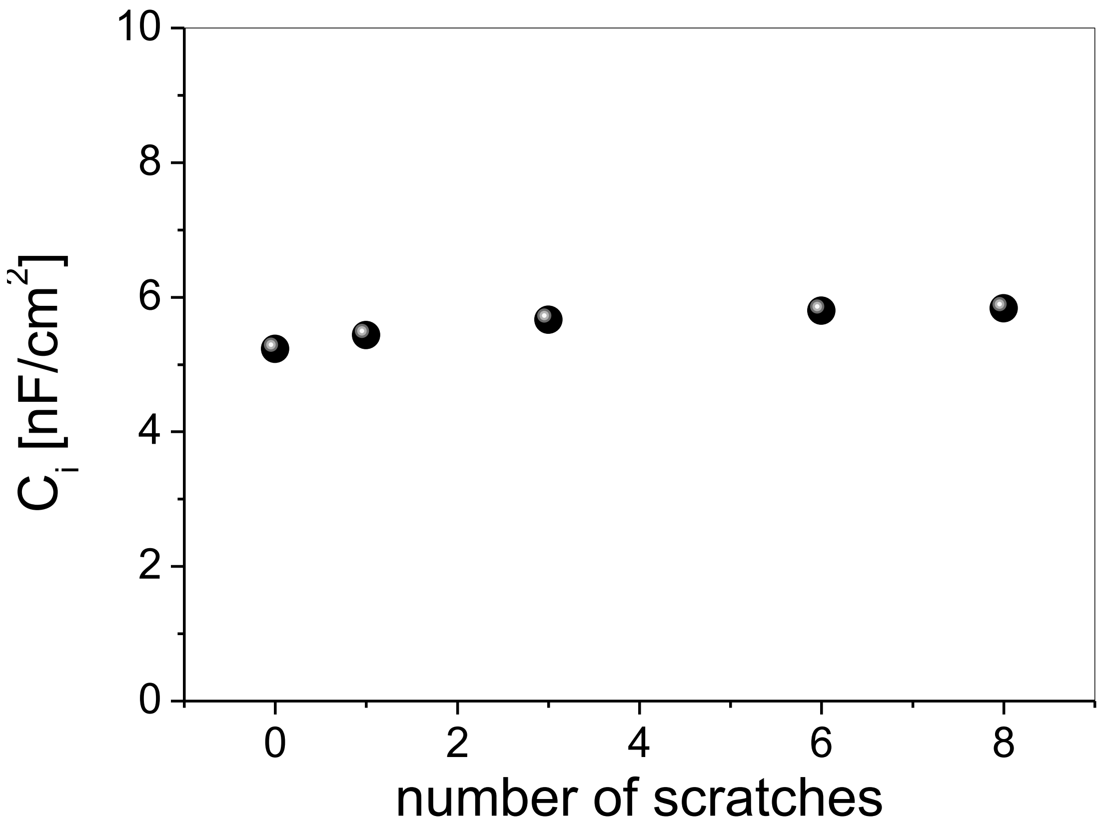

Figure S4: Capacitance *versus* number of scratches on SiNx.

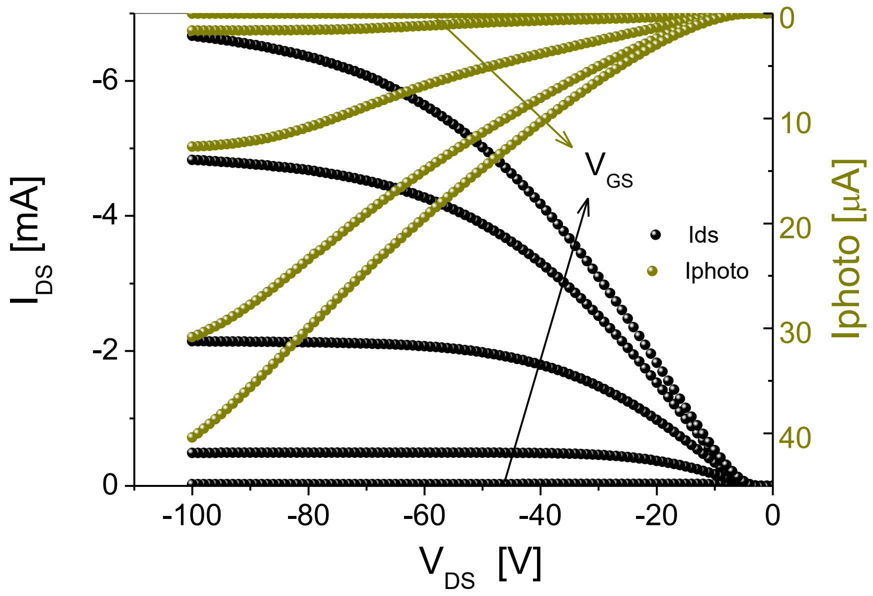

Figure S5a: Output characteristics of SY based LEFETs.

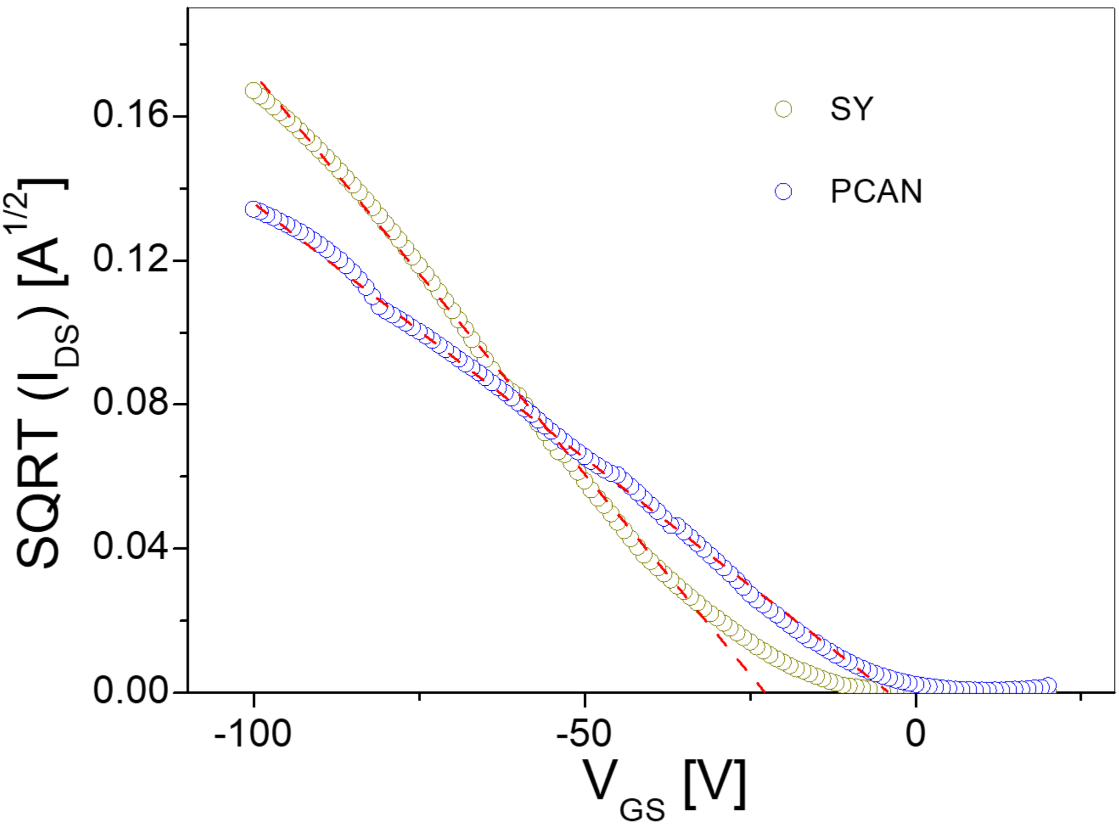

Figure S5b: Single slope linear fitting SQRT(I_{DS}) *versus* V_{GS} data of SY (yellow) and PCAN (blue) based LEFETs.

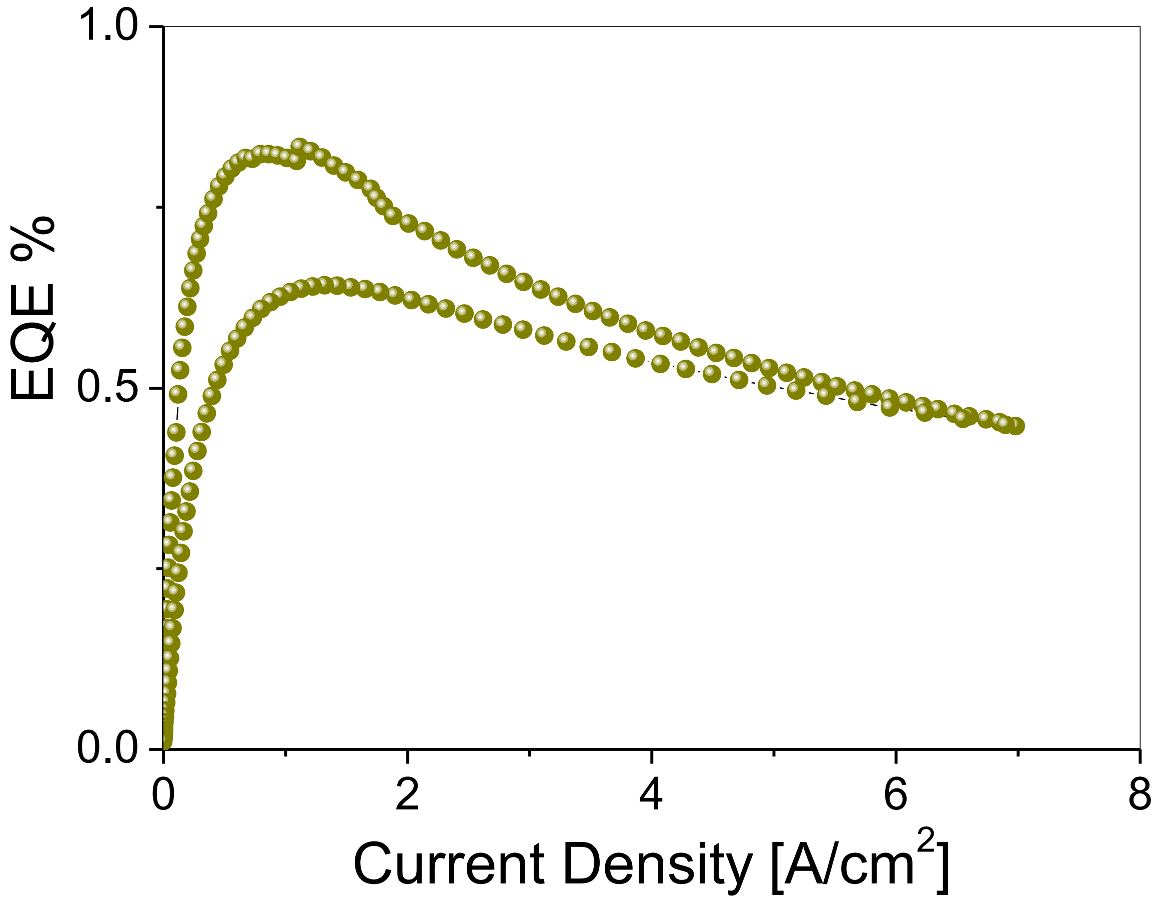

Figure S6: EQE *versus* current density of SY based LEEFTs**.**

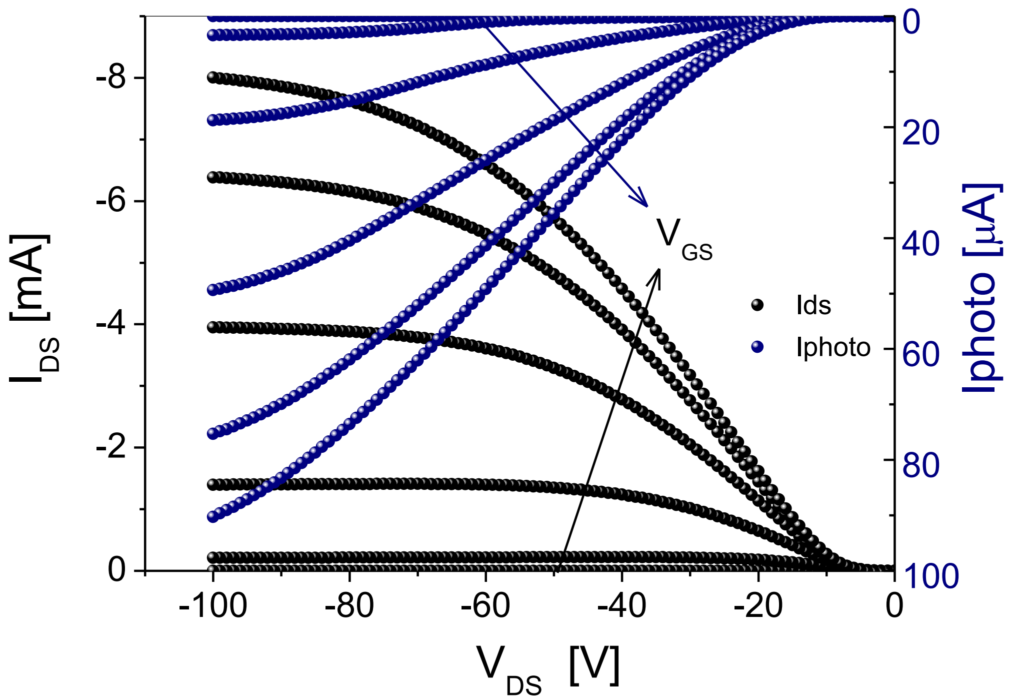

Figure S7: Output characteristics of PCAN based LEFETs.

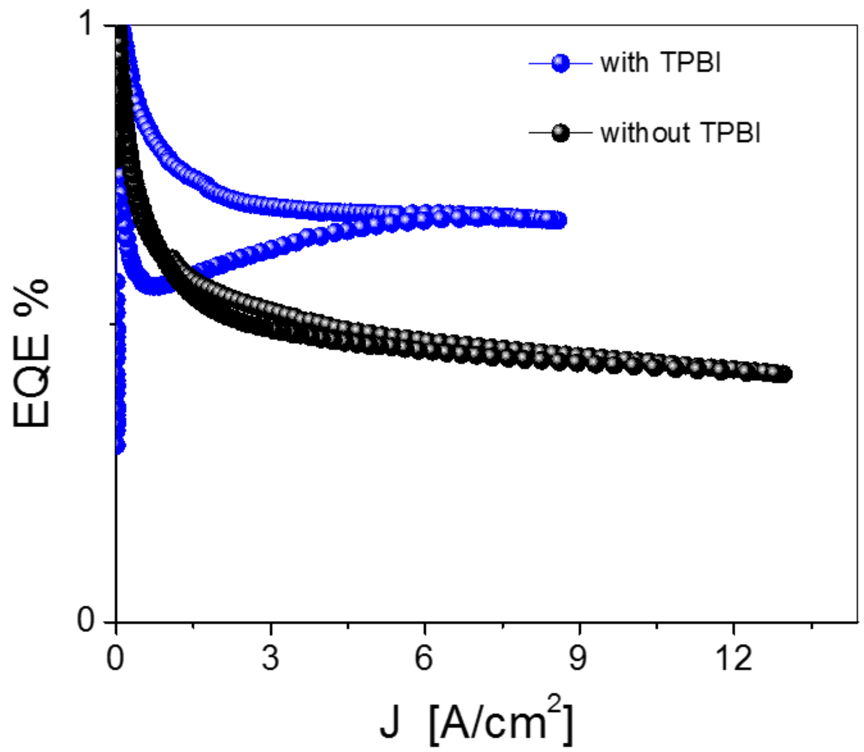

Figure S8: EQE *versus* current density (*J*) of PCAN based LEEFTs (with TPBI layer and without TPBI layer under the electrode).

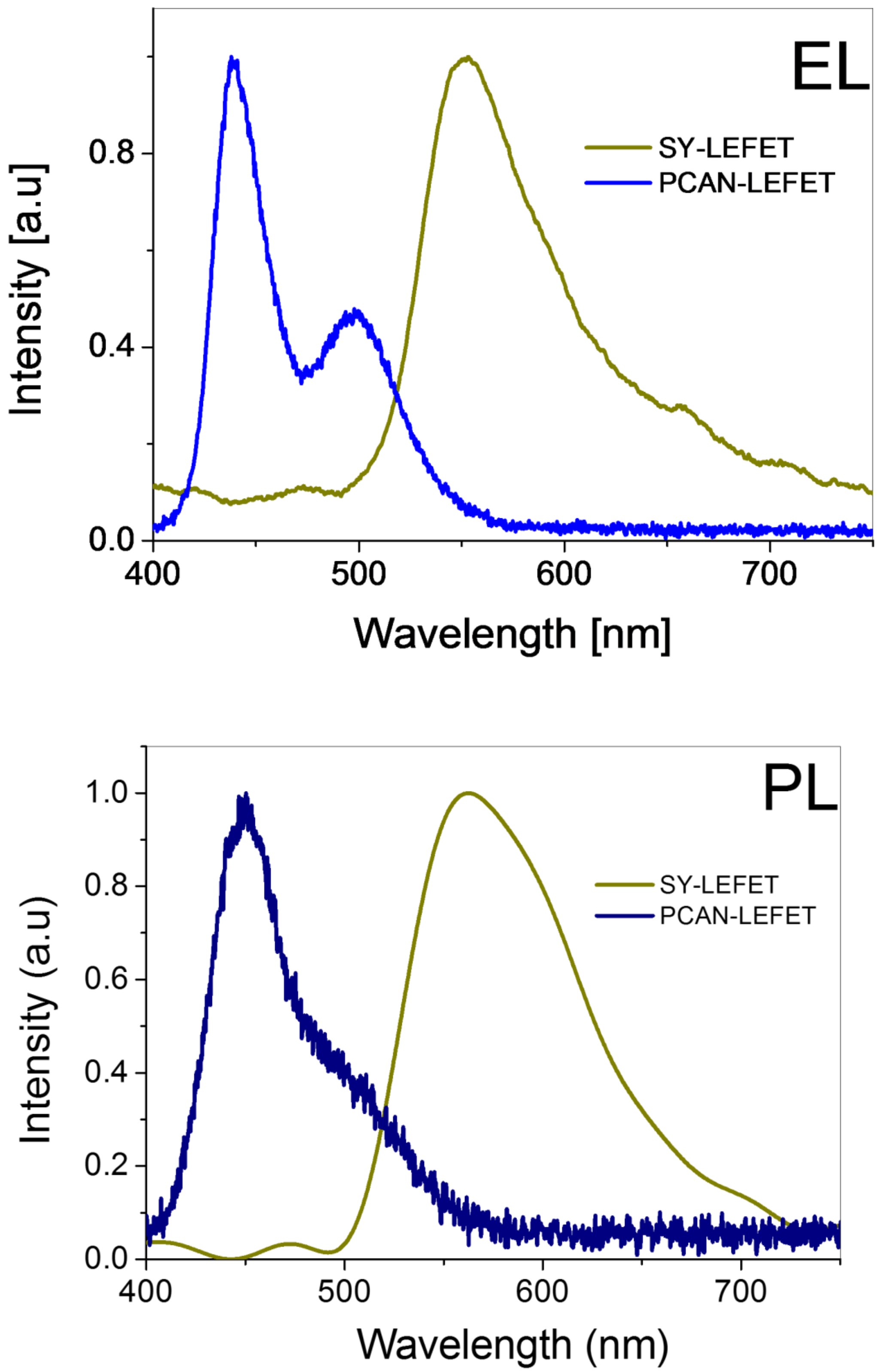

Figure S9: Electroluminescence (top) and photoluminescence (bottom) spectra of SY and PCAN based LEFETs.

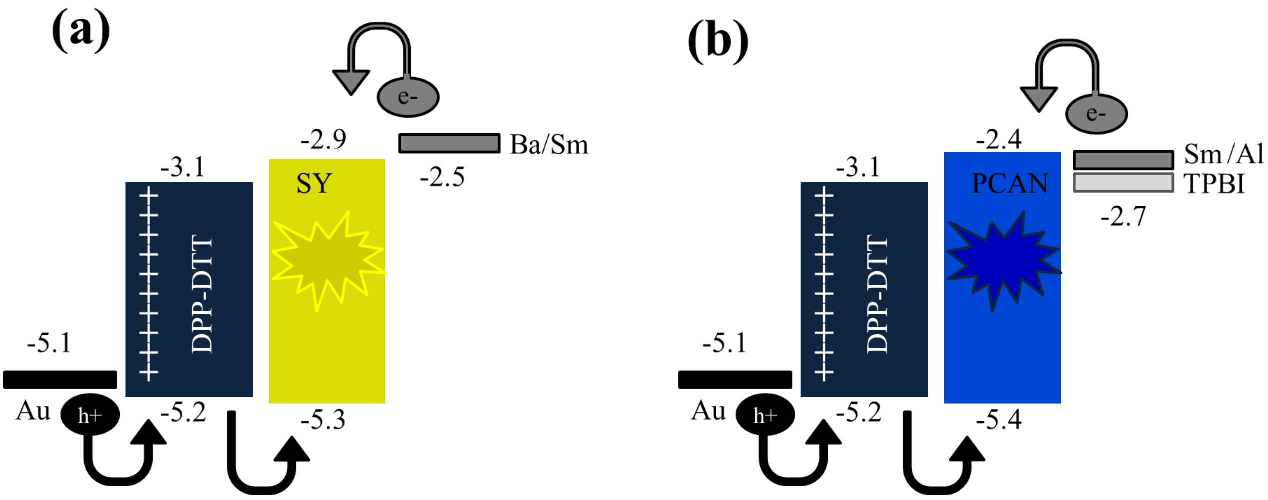

Figure S10: Charge transport and injection mechanism and their relative energy levels**:** (a) SY based LEEFTs; (b) PCAN based LEFETs.

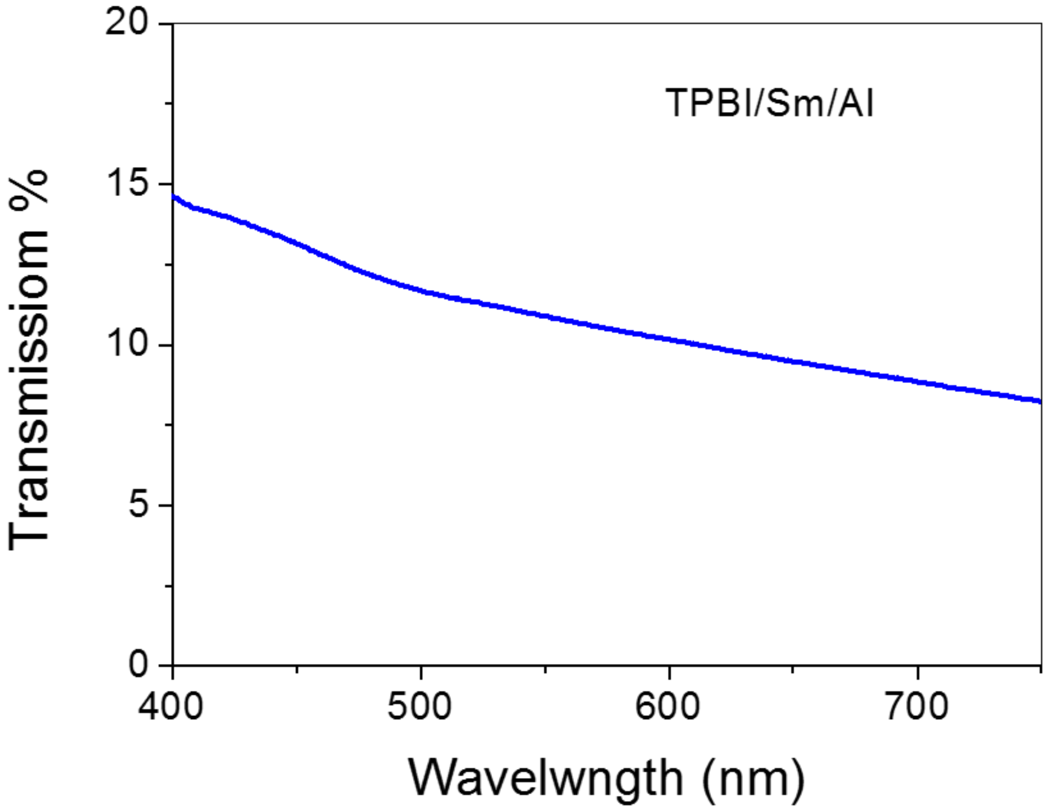

Figure S11: Transmission of the electron injecting electrode (TPBI/Sm/Al).

Table S1: Comparison with Literature.

A comparison of the results of green-yellow LEFETs, previously reported and in this study.

	This study	**Ref #1**	**Ref #2**	**Ref #3**	**Ref #4**	**Ref #5**	**Ref #6**
Device Architecture	**3 terminal 2-layer**	**3 terminal 3-layer**	**3 terminal 2-layer**	**3 terminal 2- layer**	**3 terminal 1- layer**	**3 terminal 1- layer**	**3 terminal 2- layer**
Emissive Material	**SY**	**SY**	**SY**	**SY**	**F8BT**	**Rubrene & Tetracene (Single Crystals)**	**Rubrene**
μ_{hole} **(cm^2/Vs)**	5	0.12	0.5	0.5	- (<0.001)	0.82 & 2.3	-
$\mu_{electron}$ **(cm^2/Vs)**	-	0.003	-	0.2	- (<0.001)	0.27 & 0.12	0.6
Maximum Brightness (cd/m^2)	29,000	2,100	800 @-100 V	850	8,000	800	220
EQE at maximum brightness (%)	0.4	0.06	0.08 @-100 V	0.1	4	0.002 & 0.02	0.012

Table S2: Comparison with Literature.

A comparison of the results of blue emitting organic LEFETs, previously reported and in this study.

	This study	**Ref #1**	**Ref #7**	**Ref #8**	**Ref #9**	**Ref #10**
Device architecture	**3 terminal** **2-layer**	**3 terminal** **3-layer**	**3 terminal** **1-layer**	**3 terminal** **1-layer**	**3- terminal** **1-layer**	**3 terminal** **3-layer**
Material	**PCAN**	**SPB-02T**	**EFIN**	**BSB-Me** **(single crystal)**	**P3V2** **(single crystal)**	**PFO**
Emission colour	Deep blue	Clue	blue	blue	blue	blue
μ_{hole} **(cm^2/Vs)**	7	0.1	0.000006	0.0001	0.11	0.16
$\mu_{electron}$ **(cm^2/Vs)**	-	0.004	-	0.01	0.013	-
Maximum brightness **(cd/m^2)**	9,600	816	Not reported	Not reported	Not reported	137
EQE at maximum brightness (%)	0.7	0.05	Not reported	Not reported	Not reported	0.001

References:

1. Ullah, M.; Tandy, K.; Yambem, S. D.; Aljada, M.; Burn, P. L.; Meredith, P.; Namdas, E. B. Simultaneous enhancement of brightness, efficiency, and switching in RGB organic light emitting transistors. *Adv. Mater.* **2013**, *25*, 6213.

2. Hsu, B. Y.; Seifter, J.; Takacs, C.; Zhong, C.; Tseng, H.-R.; Samuel, I. D. W.; Namdas, E. B; Bazan, G. C.; Huang, F.; Cao, Y.; Heeger, A. J. Ordered polymer nanofibers enhance output brightness in bilayer light-emitting field-effect transistors. *ACS Nano* **2013**, *7*, 2344–2351.

3. Ullah, M.; Tandy, K.; Li, J.; Shi, Z.; Burn, P. L.; Meredith, P.; Namdas, E. B. High-mobility, heterostructure light-emitting transistors and complementary inverters. *ACS Photonics* **2014**, *1*, 954–959.

4. Gwinner, M. C.; Kabra, D.; Roberts, M.; Brenner, T. J. K.; Wallikewitz, B. H.; McNeill, C.; Friend, R. H.; Sirringhaus, H. Highly efficient single-layer polymer ambipolar light-emitting field-effect transistors. *Adv. Mater.* **2012**, *24*, 2728–2734.

5. Takenobu, T.; Bisri, S. Z.; Takahashi, T.; Yahiro, M.; Adachi, C.; Iwasa, Y. High current density in light-emitting transistors of organic single crystals. *Phys. Rev. Lett.* **2008**, *100*, 066601.

6. Ullah, M., Yambem, S. D.; Moore, E. G.; Namdas, E. B.; Pandey, A. K. Singlet fission and triplet exciton dynamics in rubrene/fullerene heterojunctions: implications for electroluminescence. *Adv. Electron. Mater*. **2015**, *1*, 1500229.

7. Ke, T.-H.; Gehlhaar, R.; Chen, C.-H.; Lin, J.-T.; Wu, C.-C.; Adachi, C. High efficiency blue light emitting unipolar transistor incorporating multifunctional electrodes. *App. Phys. Lett.* **2009**, *94*, 153307.

8. Nakanotani, H.; Kabe, R.; Yahiro, M.; Takenobu, T.; Iwasa, Y.; Adachi, C. Blue-light-emitting ambipolar field-effect transistors using an organic single crystal of 1,4-bis(4-methylstyryl)benzene. *Appl. Phys. Express* **2008**, *1*, 091801.

9. Nakanotani, H.; Saito, M.; Nakamura, H.; Adachi, C. Highly Balanced Ambipolar mobilities with intense electroluminescence in field-effect transistors based on organic single crystal oligo(p-phenylenevinylene) derivatives. *Appl. Phys. Lett.* **2009**, 95, 033308.

10. Namdas, E. B.; Hsu, B. B.; Liu, Z.; Lo, S.-C.; Burn, P. L.; Samuel, I. D. W. Phosphorescent light-emitting transistors: harvesting triplet excitons. *Adv. Mater.* **2009**, *21*, 4957–4961.